Initial Results of Neutron Emission Profile Measurements in LHD Deuterium Plasmas*)

Hiroki KAWASE[1)], Kunihiro OGAWA[1,2)], Takeo NISHITANI[2)], Neng PU[1)], Sadayoshi MURAKAMI[3)], Mitsutaka ISOBE[1,2)] and LHD Experiment Group[2)]

[1)]*SOKENDAI (The Graduate University for Advanced Studies), 322-6 Oroshi-cho, Toki 509-5292, Japan*
[2)]*National Institute for Fusion Science, National Institutes of Natural Sciences, 322-6 Oroshi-cho, Toki 509-5292, Japan*
[3)]*Kyoto University, Kyoto 615-8540, Japan*

(Received 4 January 2018 / Accepted 5 October 2018)

Measurements of radial DD neutron emission profiles by the vertical neutron camera (VNC) are performed in neutral beam-heated deuterium plasmas in the Large Helical Device. The time evolution of the neutron counting rate obtained by VNC is consistent with that of the total neutron emission rate measured by the fission chamber. The radial peak position of line-integrated neutron emission profile shifts outward according to preset magnetic axis positions (R_{ax_vac}) from 3.60 m to 3.90 m. The line-integrated neutron emission profiles measured in the experiment at R_{ax_vac} of 3.60 m, 3.75 m, and 3.90 m are compared with that estimated by a calculation using FIT3D-DD code with considering the line-integration effects. The radial position of the peak in calculation is almost the same as that of in the experiment. However, the profile measured in experiment is wider than that of the calculated profile.

Keywords: LHD, deuterium plasma experiment, vertical neutron camera, neutron emission profile, FIT3D-DD

DOI: 10.1585/pfr.13.3402122

1. Introduction

The deuterium-tritium fusion reactions will be used in a future nuclear fusion reactor. Because 3.5 MeV alpha particles born in a D-T plasma play a role as a main heating source in sustaining ignited condition, good confinement of energetic particles (EPs) is required in the magnetic confinement. However, anomalous losses of EP may occur due to magnetohydrodynamic (MHD) instabilities such as energetic-particle-driven and pressure-driven MHD modes in the future fusion reactor, leading to unwanted localized heat load and/or severe damage on the first wall. Therefore, deep understanding of the classical and non-classical behaviors of EPs is important. In currently performed fusion experiments, a plasma is heated by intensive neutral beam (NB) injections. In such a condition, neutrons are mainly generated by interactions between beam ions and a thermal ion. Therefore, a neutron emission profile measurement can potentially provide the beam-ion profile and/or the radial transport of beam-ion. Because of this, the neutron camera has been used in large tokamaks producing neutrons, such as the JET [1, 2], the TFTR [3, 4], the JT-60U [5], and the MAST [6], in order to measure the spatial profile of fusion neutron emissions. Also, the radial and vertical neutron cameras in the ITER are designed to measure spatial profile of neutron emission and alpha-particle birth, fuel burnup rate, plasma positions, fuel ion temperature, and densities [7]. In previous tokamak experiments, EPs transport caused by MHD instabilities such as sawtooth and energetic-particle-continuum mode were clearly observed by using the neutron camera [8, 9].

The confinement properties of EPs have been investigated by using EPs diagnostics such as lost-fast ion probe [10] and neutral-particle analyzer [11] in hydrogen experiment phase in LHD. However, these diagnostics do not provide direct information of EPs confined in core region. The Large Helical Device (LHD) deuterium plasma experiments were carried out from March 7 to July 7, 2017. The deuterium experiments of the LHD provide a new opportunity to extend EP physics study through neutron measurements. In order to investigate radial transport of EPs, the vertical neutron camera (VNC) has been developed in LHD [12].

2. The VNC for the LHD

The VNC scheme on the LHD is shown in Fig. 1. The VNC consists of three sections: a multichannel collimator embedded in the 2.0 m thick concrete floor of the torus hall, fast-neutron scintillation detectors with eleven channels that are radially aligned, and a data acquisition system (DAQ) based on a leading edge fast-digitizer equipped with a field programmable logic circuit (FPGA).

The size of the entire multichannel collimator is 0.8 m × 1.4 m and the thickness is 1.5 m. The multichannel collimator was made of heavy concrete and stainless steel pipes

author's e-mail: kawase.hiroki@nifs.ac.jp
*) This article is based on the presentation at the 26th International Toki Conference (ITC26).

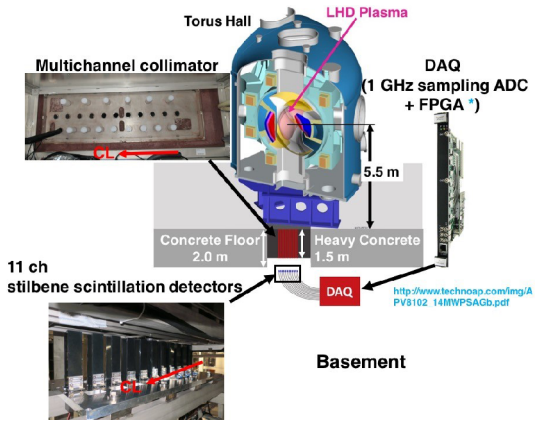

Fig. 1 Schematically drawn overview of vertical neutron camera on the LHD. The neutron collimator made of heavy concrete is embedded into the 2.0 m-thick concrete floor of the torus hall. Stilbene scintillation detector array is installed at the collimator end in the basement. DAQ equipped with 1 GHz sampling ADC and FPGA is placed in the basement. The cable length from a stilbene scintillation detector to the DAQ is 15 m.

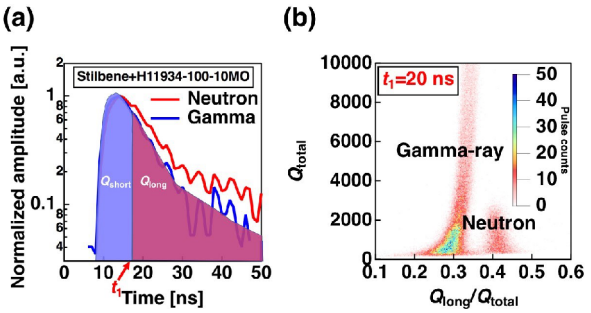

Fig. 2 (a) Pulse shape discrimination method between neutron and gamma-ray pulses. Appropriate t_1 is necessary to obtain good n-γ discrimination. (b) Result of n-γ discrimination in LHD experiment. Two peaks are clearly discriminated. A peak having large Q_{long}/Q_{total} corresponds to neutron, and the other peak is gamma-ray. Here, t_1 was set to be 20 ns.

with an inner diameter of 30 mm arranged in the radial direction. Furthermore, the distance between each neighboring pipe center axis is 90 mm. The heavy concrete of which the density is about 3.5 g/cm^3 is made from hematite (Fe_2O_3)-doped concrete. The fast-neutron detectors for the VNC consist of a stilbene scintillator with a diameter of 20 mm and a thickness of 10 mm, and a photomultiplier tube (H11934-100-10MOD: HAMAMATSU Photonics K.K.) with booster power supplies to suppress the gain shift in the high-current operation regime. The magnetic field strength on the scintillation detector position is relatively strong up to 100 mT. The magnetic shield of which length of 300 mm composed of iron with 7 mm thickness and permalloy-C with 1 mm thickness is designed based on the finite element method calculation and is applied to avoid the magnetic field effect on the photomultiplier tube. A stilbene scintillation detector was adopted as a fast-neutron detector in terms of high luminosity, fast-response, and good neutron-gamma (n-γ) discrimination capabilities. Discrimination between neutron and gamma pulses can be performed from the different decay time in the pulse shape. As shown in Fig. 2 (a), an arbitrary falling time t_1 is set appropriately in the pulse waveform. Subsequently, two peaks appear in the histogram of Q_{long}/Q_{total} from Fig. 2 (b) when Q_{long} and Q_{total}(= Q_{short} + Q_{long}) are calculated. A peak with a large value of Q_{long}/Q_{total} results from neutrons, and the other peak corresponds to gamma-rays. The DAQ (APV8102-14MWPSAGb, V_{PP} 6V, 14 bits, 2 GB DRAM: Techno-AP Co., Ltd.) is characterized by high-speed sampling (1 GHz) ADC and FPGA, which enable both online and offline n-γ discrimination, simultaneously. The neutron measurement section of VNC on the LHD can be stably operated over 1×10^6 cps to follow rapid events with good statistics on the number of pulse counts. The cross talk from the neighboring channel is evaluated by means of ^{252}Cf neutron source [13]. It is found that cross talk from the neighboring channel is around 3% as expected by three dimensional Monte Carlo neutronics code MCNP6 [14].

3. Experimental Results

3.1 Time evolution of neutron emission profile

A time evolution of line-integrated neutron emission profiles was measured with VNC in deuterium plasmas with the following parameters: the magnetic axis position in vacuum (R_{ax_vac}) of 3.60 m and the toroidal magnetic field strength (B_t) of 2.75 T. The direction of B_t is counter clockwise (CCW) from the top. Figure 3 (a) shows waveforms of plasma parameters at t from 3.0 to 5.0 s: ECH injection power (P_{ECH}), the injection power of NB (P_{NB}), line-averaged electron density (n_{e_avg}) measured with the HCN laser interferometer [15], the central electron temperature (T_{e0}) measured with the Thomson scattering diagnostic [16], and total neutron emission rate (S_n) measured with the absolutely calibrated fission chamber [17]. Here, NB1 and NB2 inject hydrogen beams whereas NB3 and NB5 inject deuterium beams. Figure 3 (b) shows the time evolution of line-integrated neutron emission profiles at t from 3.0 s to 5.0 s. Here, the time bin was set to be 0.1 s. The line-integrated neutron counting rate had maximum at major radius R of 3.72 m. The radial peak position of line-integrated neutron counting rate was similar to the position of T_{e0} measured with the Thomson scattering diagnostics. The line-integrated neutron counting rate rapidly increased when deuterium beams were additionally injected into deuterium plasmas from at $t \sim 4.4$ s.

3.2 Measurement of neutron emission profiles in various magnetic axis configurations

The line-integrated neutron emission profiles were

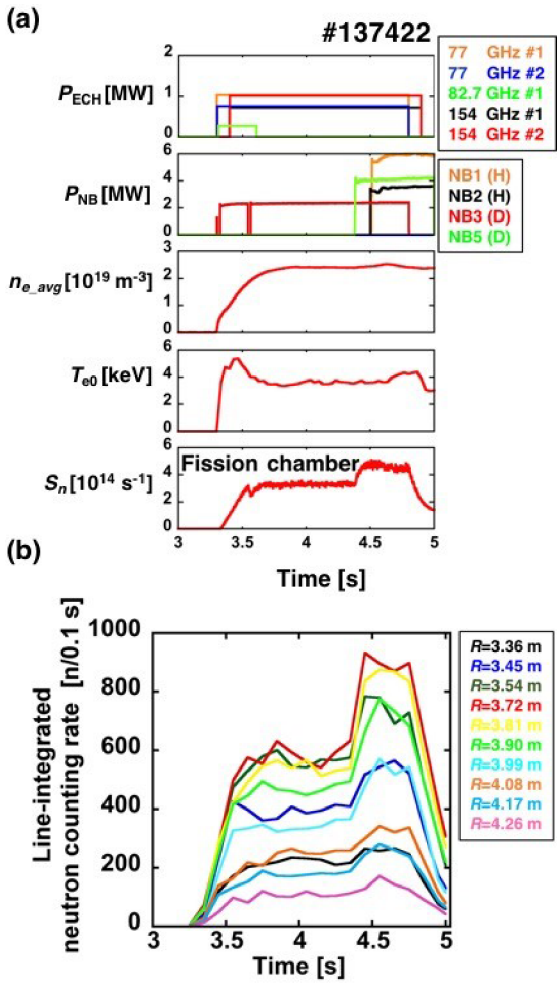

Fig. 3 (a) Waveforms of the deuterium plasma discharge in #137422. (b) Time evolutions of line-integrated neutron emission measured at various major radii.

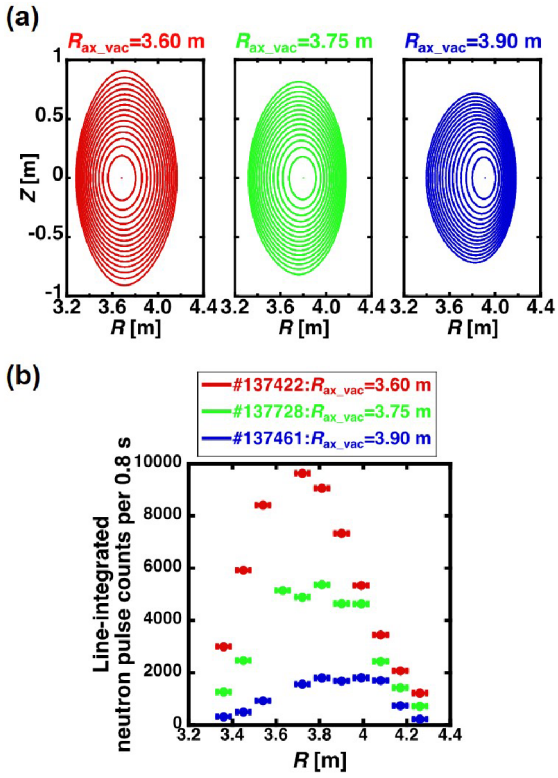

Fig. 4 (a) Magnetic flux surfaces at vertically elongated poloidal cross sections. (b) Line-integrated neutron emission profiles measured in tangential NB3 co-injected plasma with R_{ax_vac} of 3.60 m (#137422), 3.75 m (#137728), and 3.90 m (#137461). Neutron pulses were integrated for 0.8 s in this case.

measured in plasmas with R_{ax_vac} of 3.60 m, 3.75 m, and 3.90 m, respectively. In these discharges, deuterium NB3 is tangentially co-injected. Figure 4 (a) shows poloidal cross sections of the flux surface at R_{ax_vac} of 3.60 m, 3.75 m, and 3.90 m where measurements were performed. Line-integrated neutron emission profile measurements at R_{ax_vac} of 3.60 m, 3.75 m, and 3.90 m are shown in Fig. 4 (b). The red dots, the green dots, and the blue dots show the line-integrated neutron emission profiles at R_{ax_vac} of 3.60 m, 3.75 m, and 3.90 m, respectively. As can be seen, the radial peak of the profiles shifted outward with an increase of R_{ax_vac} as expected. Line-integrated neutron pulse counts increased as magnetic axis shifted inward, which indicates the confinement of EPs is improved by the inward shift of magnetic field configurations [18].

3.3 Comparison between experimental and calculation results for the line-integrated neutron emission profile

The line-integrated neutron emission profile in the three magnetic configuration of R_{ax_vac}/B_t of 3.60 m/2.75 T (CCW) (#137422), 3.75 m/2.64 T (CCW) (#137728), and 3.90 m/2.54 T (CCW) (#137461) were evaluated by FIT3D-DD code [19]. In the FIT3D-DD code, the radial neutron emission due to beam-thermal reaction is calculated using the velocity distribution of fast ions evaluated by a steady-state analytical solution of Fokker-Planck equations. The profiles of electron temperature and density as a function of the normalized minor radius (r/a) of deuterium plasma discharges in #137422, #137728, and #137461 at t = 4.0 s shown in Figs. 5 (a), 5 (b), and 5 (c) were used in the calculation by the FIT3D-DD code. Here we assumed that the radial profile of the ion temperature is the same as that of the electron temperature. In Figs. 5 (d), 5 (e), and 5 (f), the radial profiles of the beam-ion density calculated by the FIT3D-DD code are shown. The beam-ion density has a peaked profile in around the center of the plasma. In Figs. 5 (g), 5 (h), and 5 (i), the radial profiles of neutron production rate due to beam-thermal ion fusion reaction are shown. The profiles in Figs. 5 (d), 5 (e), and 5 (f) are similar to that in Figs. 5 (g), 5 (h), and 5 (i).

The profile shape has been compared. It is noted that S_n predicted by the FIT3D-DD is higher than measured S_n with the fission chamber by a factor of two as reported in ref [20]. Figures 6 (a), 6 (b), and 6 (c) show measured and

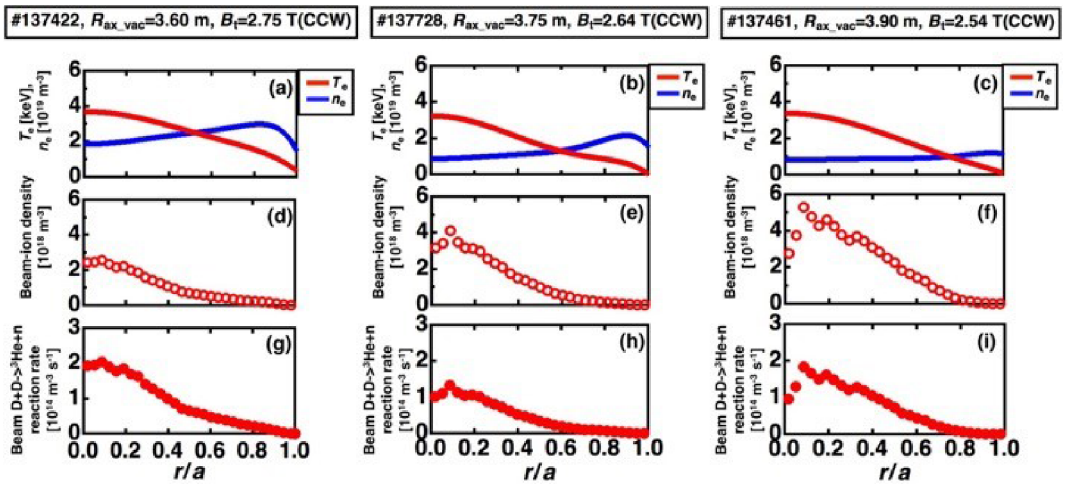

Fig. 5 (a), (b), and (c) The radial profile of deuterium plasma electron temperature and electron density in #137422, #137728, and #137461 at t = 4.0 s, respectively. The calculated radial profiles of (d), (e), and (f) the beam-ion density and (g), (h), and (i) beam-thermal fusion reaction rate are shown.

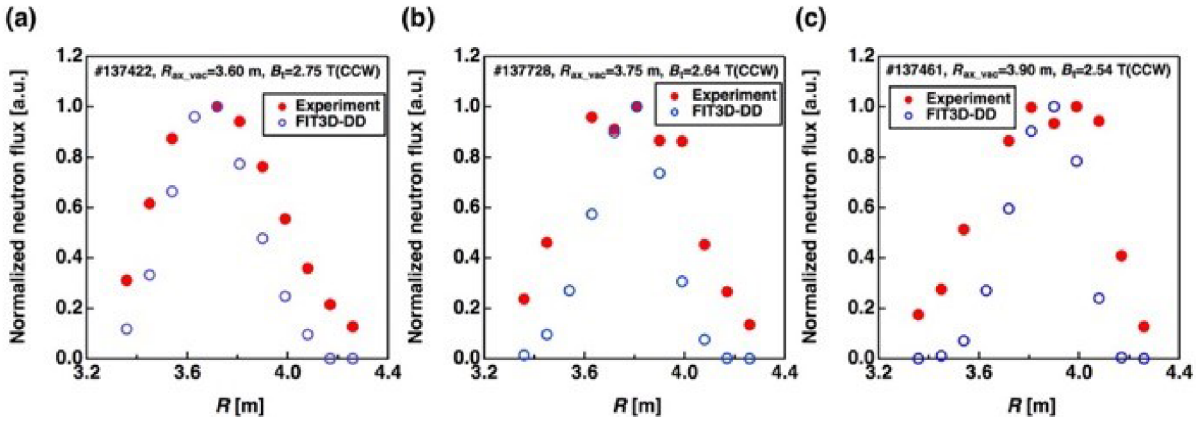

Fig. 6 Normalized line-integrated neutron emission profiles in experiment (red dots) and calculation (blue dots).

calculated line-integrated neutron emission profiles. Here, line-integrated neutron pulse counts are normalized at the peak of each profiles. These radial peak positions of experimentally measured neutron emission profile are almost the same as that of calculated profiles. However, the width of the neutron emission profile measured in experiments is wider than that of calculated profile. In case of R_{ax_vac} = 3.60 m, the full width at half maximum of the profile in experiment is 0.6 m, whereas the width in the calculation is 0.4 m. FIT3D-DD calculates neutron emission profile by assuming that the drift surface of beam ion matches the magnetic surface and beam ion has no poloidal Larmor radius. Therefore, two reasons why measured profiles are wider than calculation results are considered. One possible reason is deviation of guiding center beam ion orbit from magnetic flux surface. For example, some of helical trapped particles move from r/a = 0.2 to 0.8 for R_{ax_vac} = 3.75 m configuration. In order to take this effect into account more precisely, calculation by the Global NEoclassical Transport (GNET) code [21] is ongoing. Another possible reason is the finite Larmor radius effect. For B_t = 2.75 T and beam energy of 159 keV, the Larmor radius is 0.03 m which corresponds to approximately 5% of the minor radius of the plasma. In the future, we will perform Monte Carlo simulation including full orbit calculation, although such simulation is time consuming.

4. Summary

DD neutron emission profiles were measured by using VNC in a first deuterium campaign of LHD. The line-integrated neutron counting rate obtained by VNC showed a similar time trend to the total neutron emission rate measured by the fission chamber. The peak of the line-integrated neutron counting rate was close to the plasma center measured by the Thomson scattering diagnostics. Neutron emission profiles were measured in three different magnetic axis configurations: R_{ax_vac} of 3.60 m, 3.75 m, and 3.90 m. The peak of the line-integrated neutron emission profile shifted outward as R_{ax_vac} increased. The line-integrated neutron emission measured in R_{ax_vac}

of 3.60 m, 3.75 m, and 3.90 m are compared with that calculated based on FIT3D-DD code. It is found that the profile measured in experiments is wider than that evaluated by the calculation. Possible reasons are expected to be due to the effects of deviations of the guiding center orbit from the magnetic flux surface, the finite Larmor radius, and radial transport of beam ions. The calculation with including those effects is in progress.

Acknowledgments

This work was supported by the LHD project budgets (ULHH003, ULHH034, and ULGG801) and JSPS Grant-in-Aid for Scientific Research (B) Grant No. 26289359. This work was partly performed with the support and under the auspices of the NIFS Collaboration Research program (KOAH033).

[1] J.M. Adams *et al*., Nucl. Instrum. Methods **A329**, 277 (1993).
[2] O.N. Jarvis *et al*., Fusion Eng. Des. **34-35**, 59 (1997).
[3] A.L. Roquemore *et al*., Rev. Sci. Instrum. **61**, 3163 (1990).
[4] A.L. Roquemore *et al*., Rev. Sci. Instrum. **68**, 544 (1997).
[5] M. Ishikawa *et al*., Rev. Sci. Instrum. **73**, 4237 (2002).
[6] M. Weiszflog *et al.*, Rev. Sci. Instrum. **85**, 11E121 (2014).
[7] L. Beralot *et al.*, JINST **7**, C04012 (2012).
[8] F.B. Marcus *et al*., Plasma Phys. Control. Fusion **33**, 277 (1991).
[9] M. Ishikawa *et al*., Nucl. Fusion **45**, 1474 (2005).
[10] K. Ogawa *et al*., Nucl. Fusion **50**, 084005 (2010).
[11] M. Osakabe *et al*., Plasma Fusion Res. **5**, S2042 (2010).
[12] K. Ogawa *et al*., Rev. Sci. Instrum. **85**, 11E110 (2014).
[13] H. Kawase, "Evaluation of Spatial Resolution of Neutron Profile Monitor in LHD", 27th IEEE Symposium on Fusion Engineering, and to be published in IEEE Transactions on Plasma Science.
[14] T. Goorley *et al*., "Features of MCNP6", Supercomputing in Nuclear Applications and Monte Carlo 2013, Paris, Oct 27-31, LA-UR-13-28114 (2013).
[15] T. Akiyama *et al.*, Fusion Sci. Technol. **58**, 352 (2010).
[16] I. Yamada *et al.*, Fusion Sci. Technol. **58**, 345 (2010).
[17] M. Isobe *et al.*, Rev. Sci. Instrum. **85**, 11E114 (2014).
[18] S. Murakami *et al*., Plasma Fusion Res. **5**, 620 (2002).
[19] S. Murakami *et al*., Trans. Fusion Technol. **27**, 259 (1995).
[20] M. Osakabe *et al*., IEEE Trans. Plasma Sci. **46**, 2324 (2018).
[21] S. Murakami *et al.*, Nucl. Fusion **40**, 693 (2000).